scientific reports

Check for updates

OPEN

Machine learning-based pattern recognition of Bender element signals for predicting sand particle-size

Yong-Hoon Byun[1], Juik Son[1], Jungmin Yun[2], Hyunwook Choo[3] & Jongmuk Won[4]✉

This study explores the potential of integrating bender element signals with a convolutional neural network (CNN) to predict the particle size distribution of relatively uniform sand. A one-dimensional CNN analyzed time-series signals from bender elements across four sand types with particle sizes ranging from 0.5 to approximately 7 mm, under vertical stresses of 10, 50, and 150 kPa in three different cutoff frequencies (10, 50, and 100 kHz). The CNN architecture included convolutional layers augmented with batch normalization and ReLU activation functions, optimized through Bayesian techniques to enhance prediction accuracy. Experimental results demonstrated that higher stresses increased resonant frequencies and reduced arrival times of shear waves, with minor dependencies on soil type. Nevertheless, the developed CNN model well classified the four sand types at a given vertical stress and cutoff frequency, implying that the unique pattern of each sand type can be satisfactorily captured by the CNN algorithm. Overall, the framework shown in this study demonstrates that the bender element (or pattern of receiving shear wave signals) with the CNN model can be used in monitoring real-time variation of sand particle size.

Keywords Bender element, Convolutional neural network, Vertical stress, Cutoff frequency, Sand particle size

Bender elements, which comprise a central metal shim and two piezoelectric material sheets, are transducer designed to generate and detect shear waves using the piezoelectric effect. Since it is known that the bender elements exhibit superior coupling with granular materials, they have found extensive application in the assessment of shear waves in granular materials, both in controlled laboratory settings and in field conditions. Many researchers have used bender elements in laboratory experiments, including triaxial, direct shear, and oedometer tests[1–4]. Furthermore[5], horizontally installed several bender elements at different heights within a sand layer to monitor shear waves propagated during liquefaction. In field applications[6], introduced a field probe incorporating bender elements to characterize shear waves in clay layers.

Shear wave velocity can be determined by using a pair of bender elements to measure shear waves. One element acts as the sender, and the other serves as the receiver. After activating the input signal, the time interval between the rising edge of the input signal and the endpoint of the first small bump of the output signal is regarded as the first arrival time. The shear wave velocity is then calculated by dividing the travel distance between the two elements by the first arrival time. While bender elements have been widely used in clayey and sandy soils, recent studies have demonstrated their applicability in geotechnical engineering such as assessing stiffness characteristics of geogrid-reinforced aggregates during repeated load triaxial tests and in unbound aggregate layers under field conditions[7–10], characterizing propagation of shear wave through soils[11,12], and assessing shear modulus of soil-rubber mixtures[13,14].

The convolutional neural network (CNN) is one of the deep learning models, which is documented as an efficient algorithm for pattern recognition. Therefore, CNN has been widely used in many engineering applications such as structural damage identification[15–18], slope stability[19–21], seismic response prediction[22,23], and soil

[1]Department of Agricultural Civil Engineering, Kyungpook National University, 80 Daehak-ro, Buk-gu, Daegu 41566, Republic of Korea. [2]Department of Civil and Environmental Engineering, University of Ulsan, Daehak-ro 93, Nam-gu, Ulsan 680-749, Republic of Korea. [3]Department of Civil and Environmental Engineering, Hanyang University, Seoul 04763, Republic of Korea. [4]Department of Civil, Earth, and Environmental Engineering, Ulsan National Institute of Science and Technology (UNIST), UNIST-gil 50, Ulju-gun, Ulsan 44919, Republic of Korea. ✉email: jwon@unist.ac.kr

properties[24–26]. The abovementioned studies successfully developed CNN models with good performance (i.e., good accuracy of classification). Although many previous studies showed the prediction of soil properties (i.e., hydraulic conductivity, soil water characteristics curve, shear strength) using many types of regression-based machine learning models (random forest, extreme gradient boosting, decision tree)[27–32], the classification model would be required if the prediction of soil properties are achieved by pattern recognition. The abovementioned regression and classification machine learning model to predict soil properties provided reliable prediction models, but estimating soil properties through bender element signals has not been documented.

The particle size of soil is one of the most important spatially variable soil properties because of its ability to obtain insight into soil behavior from measured particle sizes (or particle size distribution). When the soil samples are available, particle sizes of soil are relatively easy to measure in the laboratory because it is not dependent on soil disturbance unlike other macroscale soil properties (e.g., shear strength, hydraulic conductivity, and soil stiffness)[33–35]. Therefore, many studies investigated the estimation of soil hydraulic properties (e.g., hydraulic conductivity and soil water characteristics curve) from measured particle sizes (estimating difficult-to-measure properties from easy-to-measure properties)[36–38]. However, the non-destructive evaluation of particle sizes at the construction site is relatively challenging, which is occasionally required as the soil sampling is not always available.

The automatically learned hierarchical features of CNN enable providing good classification accuracy by efficient training of data with complex patterns. This indicates the chance of developing a CNN model from the pattern of bender element signals for predicting soil properties. Therefore, this study aims to evaluate the chance of classifying sand type (or particle size of sand) using the bender element signals combined with CNN. The bender element signals were obtained in laboratory for training the CNN model and the performance of the developed CNN model is discussed. In addition, the potential applications of the developed framework in this study in particle size-related soil properties are also discussed.

Materials and methods

Materials

Four types of sand (K1, K2, K3, and K5) were selected for bender element experiments. As seen in particle size distributions (Fig. 1) and pictures of sand (Fig. 2), all sands selected in this study were relatively uniform where the coefficient of uniformity (C_u) < 2. The roundness of four selected sands was higher than 0.7 (evaluated by image analysis of sand particles), which indicates that all sands used in this study can be classified as rounded sand. The properties of sands used in this study are summarized in Table 1.

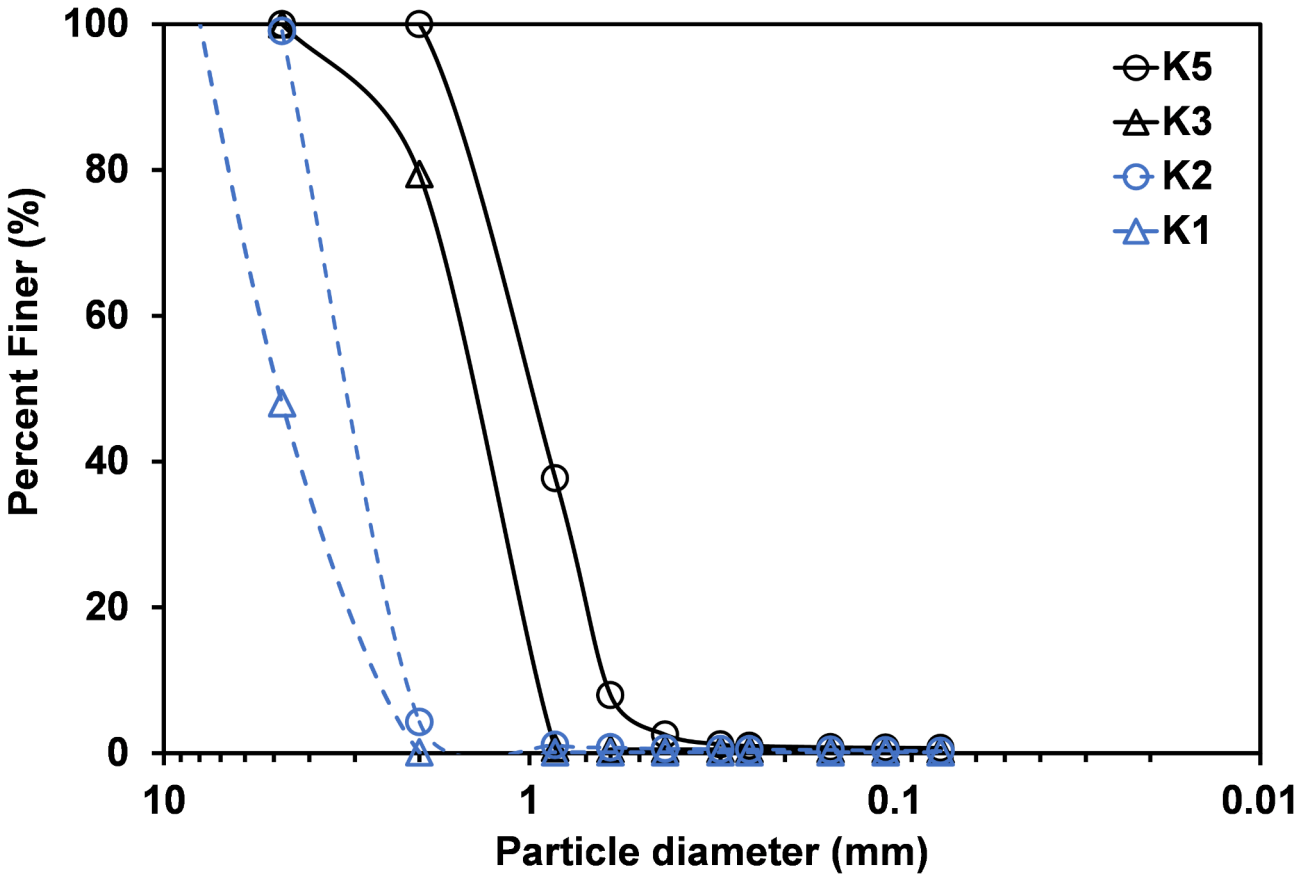

Fig. 1. Sieve analysis of K1, K2, K3, and K5 sand used in bender element experiments.

Fig. 2. Pictures of four sands used in the bender element experiments.

Notation	Property	Testing method	K1	K2	K3	K5
G_s	Specific gravity	ASTM D854	2.65	2.65	2.65	2.65
e_{max}	Maximum void ratio	ASTM D4253	0.956	0.824	0.845	0.972
e_{min}	Minimum void ratio	ASTM D4254	0.728	0.753	0.728	0.735
d_{50} (mm)	Median particle size	ASTM D422	4.8	3.4	1.7	0.83
C_u	Coefficient of uniformity	–	–	1.55	1.45	1.45
R	Roundness	–	0.748	0.768	0.757	0.813

Table 1. Properties of sand used in this study.

The four types of sand used in this study represent particle sizes ranging from 0.5 to ~7 mm, which corresponds to particle sizes of coarse and medium sands. In addition, the uniform particle size distributions of the four sand types (Fig. 1) imply that the pattern of bender element signals used in the training CNN model likely represents d_{50} of sand.

Experimental setup for training dataset

The sand specimens were prepared in a cylindrical confining cell with inner dimensions of 136 mm in diameter and 180 mm in height, as shown in Fig. 3. The oven-dried sand was placed in the cell by using the pluviation method. A pair of bender elements was located at a height of 70 mm from the bottom plate. One bender element, connected to a signal generator, transmitted elastic waves through the sand specimen. For that, a square input signal with an amplitude of 10 V and a frequency of 20 Hz was used. The other bender element detected the elastic waves, and the output signals, filtered within a specific frequency range, were recorded on an oscilloscope. For each type of sand, three different vertical stresses of 10, 50, and 150 kPa were applied to the top of the specimen. For each vertical stress, three cutoff frequencies of 10, 50, and 100 kHz were used for a low-pass filter, while the cutoff frequencies for a high-pass filter were set to 500 Hz. A total of 115 signals were saved for each vertical stress in a specific type of sand. Note that the three vertical stresses selected in this study were to simulate sand in a shallow depth, which is consistent with the range of stress levels in the literature[39,40].

Experimental setup for model validation

To assess the ability to apply the developed framework in the field, the penetration device with bender elements was designed to simulate field experimental conditions in the laboratory (Fig. 4). The device was penetrated the K1 sand medium to obtain bender element signals throughout the depth of ~500 mm, which was used as input signals in the developed CNN model. The validation result with field applicability of the developed framework in this study is discussed in Sect. 4.4. Note that the sand in Fig. 4a was prepared using the pluviation method, which is consistent with the preparation method for cylindrical cell.

Convolutional neural network

Database construction and scenarios of model development

The one-dimensional CNN was used to classify the sand type from the time-series bender element signals. A total of 460 datasets with 115 datasets for each type of sand in each scenario were applied to train the CNN model for given vertical stress and frequency. The CNN models were developed for nine scenarios (Table 2) to investigate the impact of vertical stress and frequency on the performance of CNN models. In each scenario, the dataset was randomly split into 368 and 92 datasets for training and test datasets (Fig. 5) based on the split ratio of 80:20. Note that CNN was selected in this study because it is one of the most common machine learning algorithms for pattern recognition of signals and images as found in the literature[41–46].

The raw bender element signals consist of 26,987 data points in each dataset during the measurement time of approximately 27 ms. However, training raw datasets are computationally expensive because of the high number of data points (10,578,904 data points for 392 training datasets). Therefore, datasets were filtered from the elapsed time = 0–4 ms (4,000 data points) in training CNN models in this study (Fig. 5). As seen in Fig. 5, filtered datasets showed unique patterns of signals for four sands, which implies that the filtered datasets can

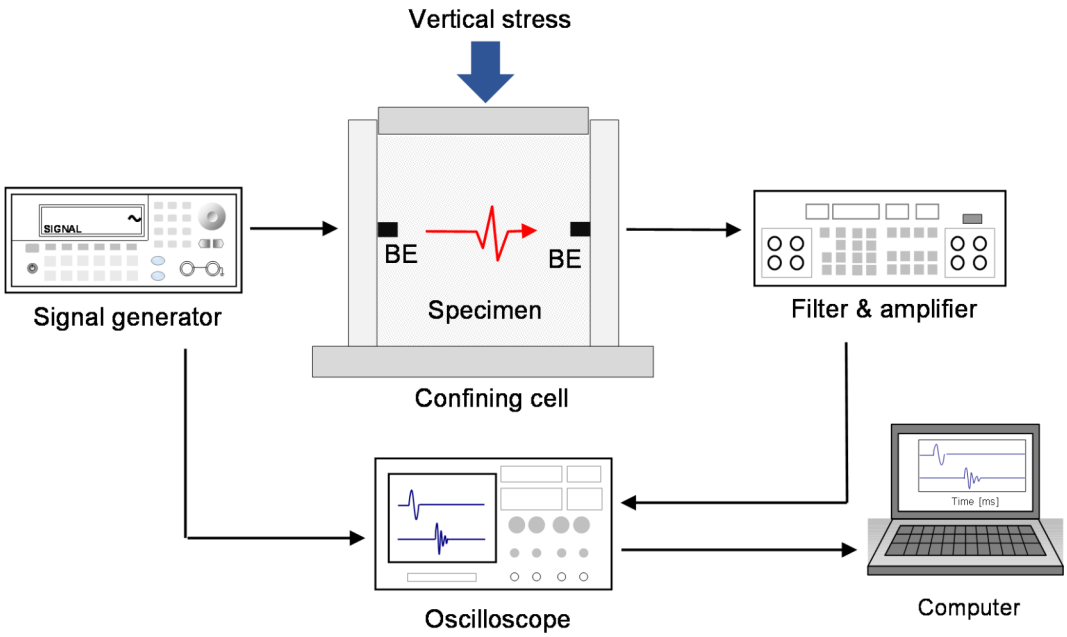

Fig. 3. A schematic of experimental setup.

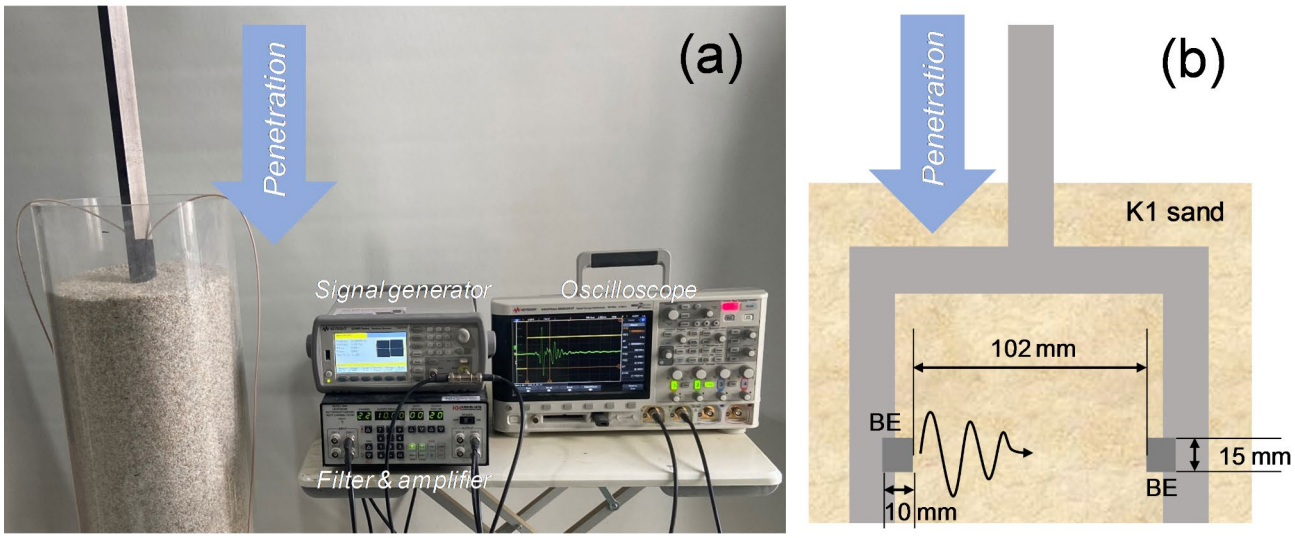

Fig. 4. A schematic of experimental setup for model validation (**a**) and designed penetration device (**b**).

Scenario no.	Vertical stress (kPa)	Cutoff frequency for lowpass filtering (kHz)
1	10	10
2		50
3		100
4	50	10
5		50
6		100
7	150	10
8		50
9		100

Table 2. Scenarios of CNN models.

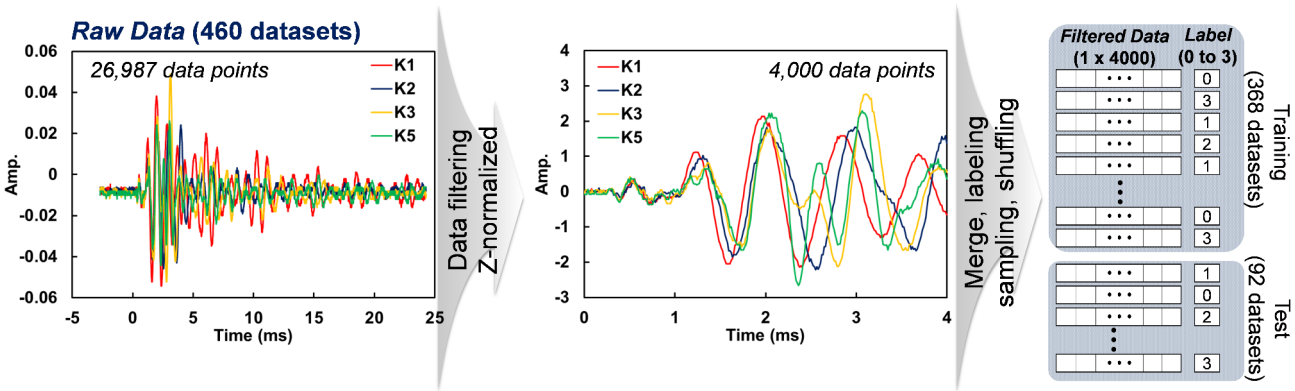

Fig. 5. Schematic drawing of data preprocessing.

effectively classify the sand type by the CNN model. The z-normalization was adopted to prevent downgrading of model performance caused by the various ranges of amplitude values[47]. The labels of the dataset for K1, K2, K3, and K5 sands were standardized as 0, 1, 2, and 3 respectively. A schematic illustration of data preprocessing is presented in Fig. 5.

Structure of 1D CNN model

Three convolutional layers were applied for the structure of one-dimensional CNN in this study. N_d (number of data in each dataset) × 1 of data points was convoluted through N_f (number of filters) filters using Relu function and batch normalization. The filtered layers by N_f were averaged after N_d × 1 data points passed through the three convolutional layers. The softmax function yielded the probability of classifying four sand types, which enables classifying the sand type for given signals as the sand type with the maximum probability. A schematic illustration of the 1D CNN structure selected in this study is presented in Fig. 6.

Hyperparameter tuning of 1D CNN model

In this study, N_f and kernel sizes of three convolutional layers were tuned during the training phase to obtain the best accuracy. The search space of N_f and kernel sizes were selected as [1, 100] and [1, 10] respectively, which are typical ranges for CNN models. Bayesian optimization tuning technique was selected with the validation accuracy during training being selected as the objective function for hyperparameters tuning. The best N_f and kernel size for each CNN model were recorded and the model accuracy for test datasets was evaluated using the best N_f and kernel size. Note that the accuracy of the CNN model without hyperparameter tuning (default N_f and kernel size were 64 and 3 respectively) was lower than 0.7, indicating that the tuning of hyperparameters is essential to develop a reliable CNN model for predicting sand type.

Performance measurement

The performance of CNN models for nine scenarios was assessed by categorical accuracy, which represents the sum of true positive divided by the total number of test datasets. In addition, precision, recall, and f1 score (harmonic mean of precision and recall scores) were also evaluated to assess the proportion of true positive predictions among all positive predictions, true positive predictions among all actual positive cases, and the balance between sand classes respectively. The average of four precision, recall, and f1 scores were evaluated in each CNN model.

Because the performance of one CNN model in a given scenario is limited to the specific split of training and test datasets, one hundred CNN models (training and test datasets were randomly selected) for each scenario were developed in this study to evaluate the uncertainty of performance and to provide the reliable performance of developed CNN models. The mean and standard deviation of performance-related values (accuracy, precision, recall, and f1 scores) were evaluated for each scenario.

The pattern of bender element signals can be also captured at a higher time interval than raw signals (time interval (Δt) = 1 μs). Therefore, the downsizing factor (F_d) was applied in this study to assess the optimal time interval of signals for good performance with low training time. For example, F_d = 2 represents sampling every two data points from the raw dataset (Δt = 2 μs). The accuracy and training time of one hundred CNN models at F_d = 1, 5, 10, 50, 100, 500, and 1000 were evaluated in this study.

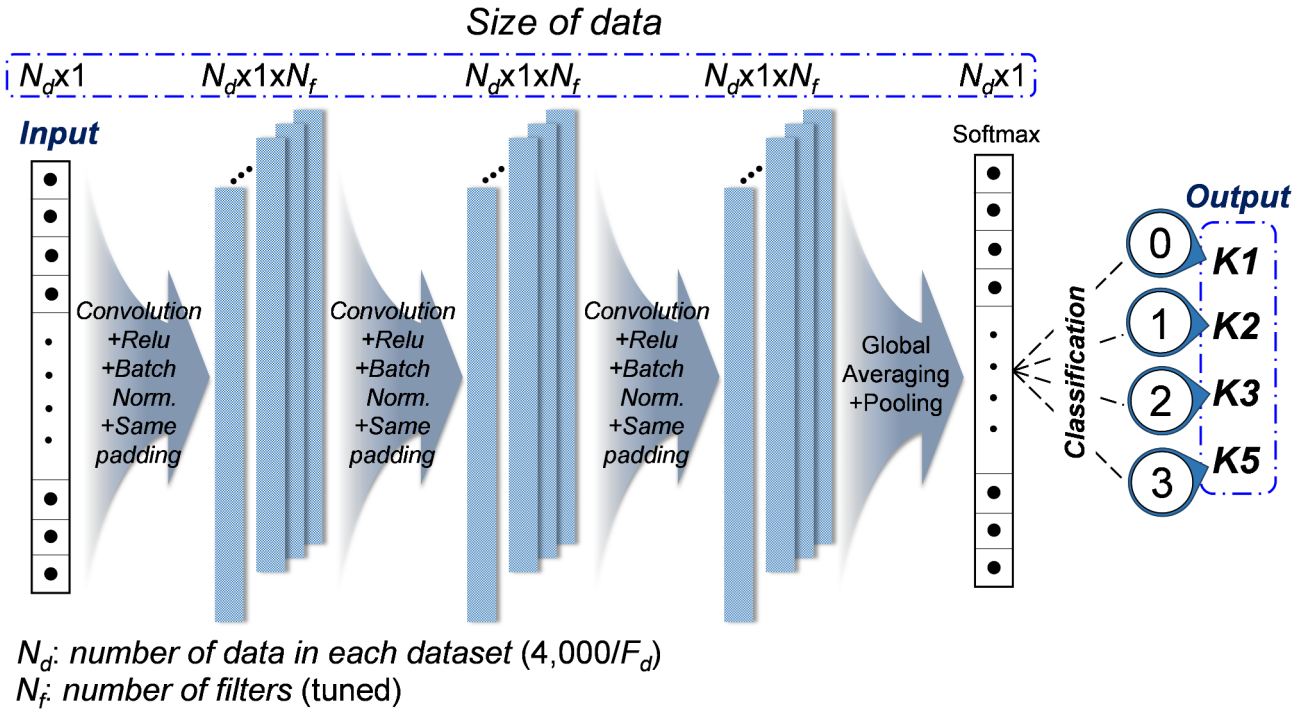

Fig. 6. Structure of convolutional neural network used in this study.

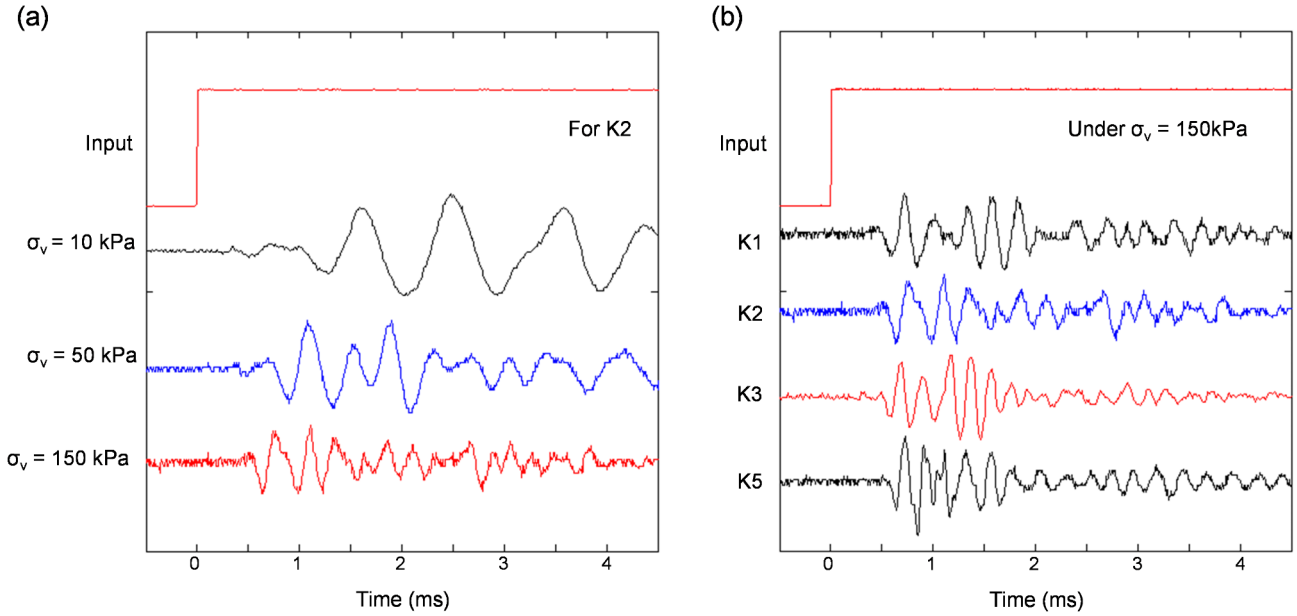

Fig. 7. Typical bender element signals along (**a**) vertical stress and (**b**) sand type.

Sand type	Vertical stress (kPa)	Cutoff frequency for lowpass filtering (kHz)		
		10	50	100
K1	10	82.0	84.4	85.1
	50	150.8	159.2	159.2
	150	165.2	174.3	175.9
K2	10	79.2	81.4	81.4
	50	112.9	116.8	116.8
	150	189.4	198.6	203.6
K3	10	77.0	79.7	79.7
	50	153.6	159.7	162.9
	150	173.3	185.1	185.1
K5	10	80.3	68.7	68.3
	50	142.5	150.0	121.8
	150	162.4	171.2	165.2

Table 3. Shear wave velocities (unit in m/s) for four sands under three vertical stresses and cutoff frequencies.

Results and discussion

Experimental observations

Figure 7 shows the typical waveforms of output signals along the vertical stress changes, in comparison to the input signals. A cutoff frequency of 100 kHz was selected for the output signals presented in Fig. 7 to prevent distortion of the original waveform caused by lowpass filtering[7], resulting in the presence of undesired high-frequency noise in the output signals. Figure 7a demonstrates that for K2, the resonant frequency of shear waves increases with the vertical stress. In addition, the output signals under higher vertical stress exhibit shorter first arrival times of shear waves. As presented in Fig. 7b, under a vertical stress of 150 kPa, the patterns and first arrival times of shear waves show a slight dependence on the soil type. It should be noted that the compressional wave reflected from the cell wall was detected earlier than the first arrival time of shear waves, which may interfere with accurately determining the first arrival time of shear waves[39,48]. The shear wave velocities calculated for four types of sand were summarized in Table 3.

Performance of CNN models (Fd = 1)

Figures 8 and 9 illustrate the confusion matrix of developed 100 CNN models for training and test datasets, respectively. As seen in Figs. 8 and 9, the developed CNN models well-classified sand type in all scenarios, which are represented by the high mean values in a diagonal direction. In addition, the low standard deviation values in a diagonal direction shown in Figs. 8 and 9 indicate good repeatability and reliability of developed CNN models

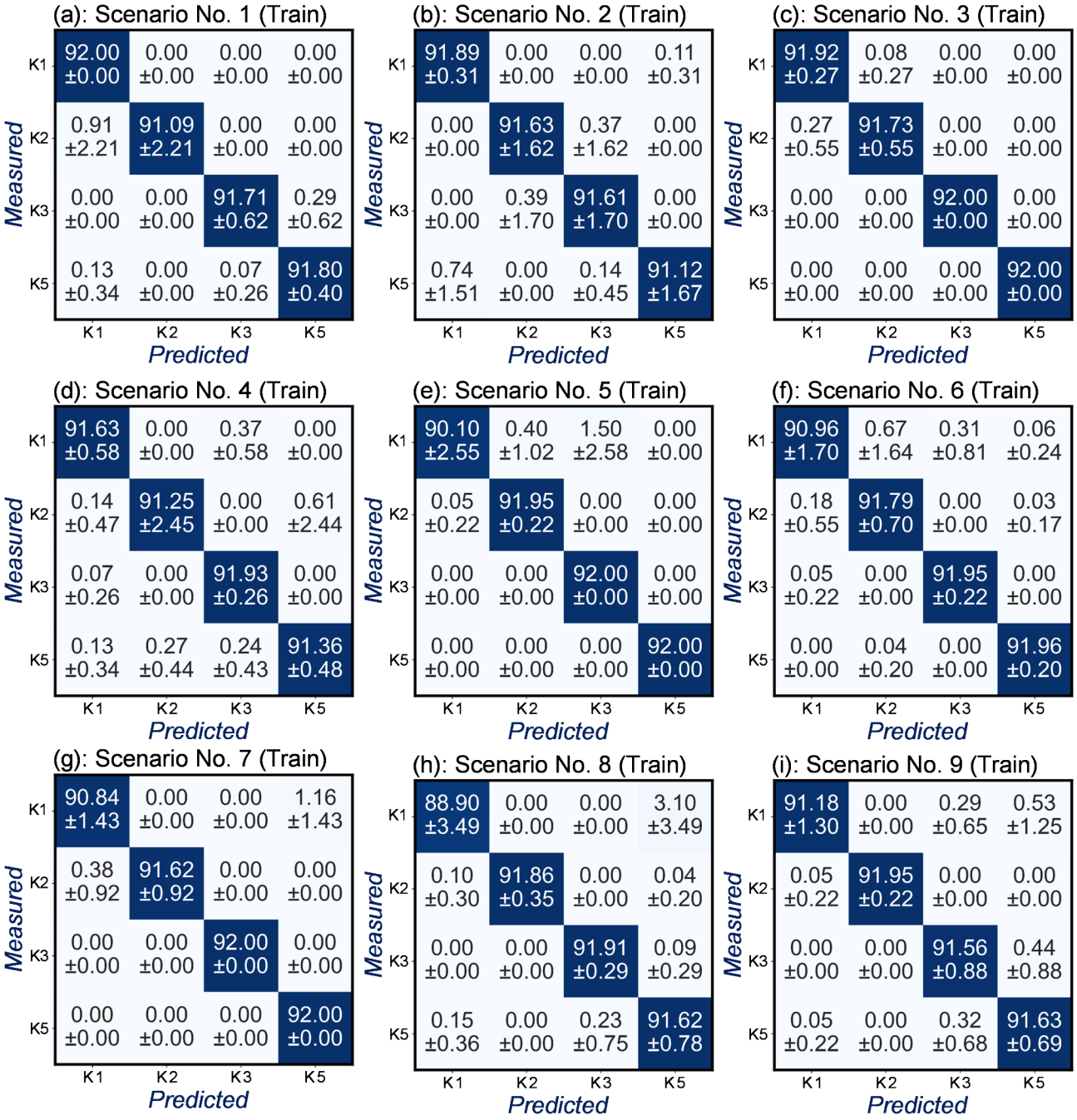

Fig. 8. Confusion matrix of 100 CNN models (mean ± standard deviation) for training datasets ($F_d = 1$).

in this study. Therefore, the developed CNN model in this study can be used to predict the sand type (or the particle size of sand) without almost no underestimation or overestimation of the particle size of sand. The good performance of developed CNN models in all scenarios implies that the good classification of sand type can be achieved in a wider range of vertical stress and cutoff frequency for lowpass filtering.

Because the high mean values in a diagonal direction were obtained, similarly high mean accuracy, precision, recall, and f1 scores were obtained for all scenarios as shown in Table 4. This implies that the developed CNN models show a well-balanced high level of accuracy in predicting sand type. In addition, an extremely low difference in mean accuracy between training and test datasets suggests the good generalization capacity of the developed CNN models.

Figure 10 illustrates the mean and standard deviation of two tuned hyperparameters (number of filters and kernel size) for three convolutional layers. As seen in Fig. 10, tuned hyperparameters for 100 CNN models showed high variability with no trend as a function of vertical stress and frequency. In other words, an optimal number of filters and kernel size cannot be determined for predicting sand size from bender element signals. The high variability hyperparameters imply that the best hyperparameters were solely dependent on the training

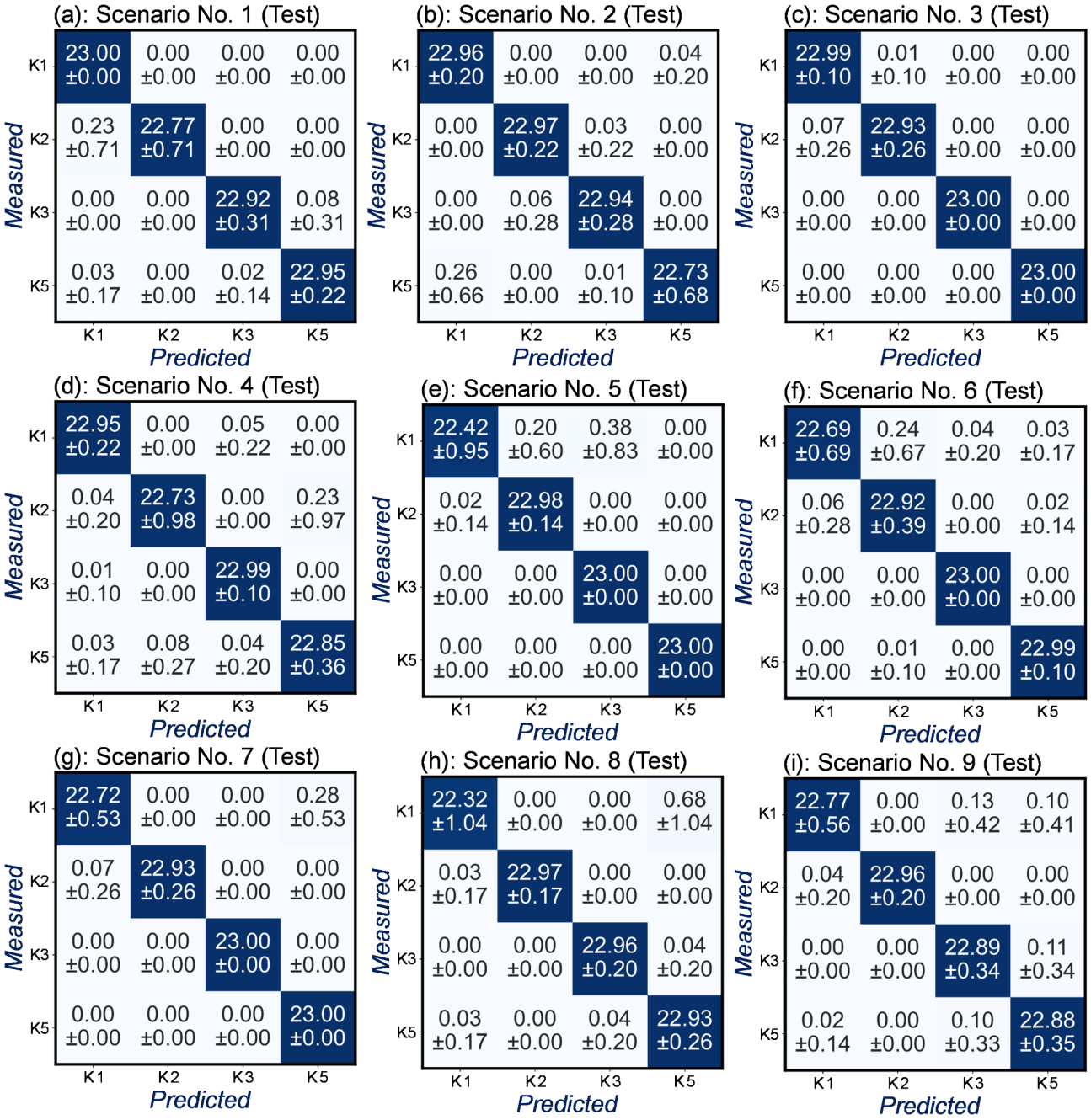

Fig. 9. Confusion matrix of 100 CNN models (mean ± standard deviation) for test datasets ($F_d = 1$).

datasets. Because the pattern and amplitude of measured bender element signals for a given sand type in this study are similar, it can be inferred that the optimal number of filters and kernel size of CNN models were extremely sensitive to the pattern of training datasets. In addition, the increase in the classification accuracy from ~ 0.7 to 0.99 after hyperparameter tuning indicates the necessity of including the process of hyperparameter tuning in model development.

Impact of Fd on performance of CNN models Fd

Figure 11 shows the accuracy of 100 CNN models at $F_d = 1$ (original dataset), 5, 10, 50, 100, 500, and 1000. In addition, the training time of 100 CNN models corresponding to Fig. 11 is also presented in Fig. 12. As seen in Fig. 11, the accuracy of CNN models decreased as F_d increased, which is more or less intuitive as the higher number of data can more effectively capture the pattern of signals. Nevertheless, it is notable that the accuracy values > 0.98 were obtained when $F_d < 500$ (corresponding to 9 data points in each dataset), whereas relatively low accuracy was obtained for $F_d = 1000$ (e.g., mean accuracy = 0.788 for scenario No. 1 (Fig. 11a). This suggests that the low number of data points by preprocessing can provide the accurate prediction of sand type with

Scenario no.	Accuracy		Precision		Recall		F1 score	
	Training	Test	Training	Test	Training	Test	Training	Test
1	0.996 ± 0.006	0.996 ± 0.009	0.996 ± 0.006	0.996 ± 0.008	0.996 ± 0.006	0.996 ± 0.009	0.996 ± 0.006	0.996 ± 0.009
2	0.995 ± 0.012	0.996 ± 0.009	0.995 ± 0.012	0.996 ± 0.008	0.995 ± 0.012	0.996 ± 0.009	0.995 ± 0.012	0.996 ± 0.009
3	0.999 ± 0.002	0.999 ± 0.003	0.999 ± 0.002	0.999 ± 0.003	0.999 ± 0.002	0.999 ± 0.003	0.999 ± 0.002	0.999 ± 0.003
4	0.995 ± 0.006	0.995 ± 0.011	0.995 ± 0.006	0.995 ± 0.010	0.995 ± 0.006	0.995 ± 0.011	0.995 ± 0.006	0.995 ± 0.011
5	0.995 ± 0.007	0.993 ± 0.010	0.995 ± 0.006	0.994 ± 0.009	0.995 ± 0.007	0.993 ± 0.010	0.995 ± 0.007	0.993 ± 0.010
6	0.996 ± 0.005	0.996 ± 0.009	0.996 ± 0.005	0.996 ± 0.008	0.996 ± 0.005	0.996 ± 0.009	0.996 ± 0.005	0.996 ± 0.009
7	0.996 ± 0.004	0.996 ± 0.006	0.996 ± 0.004	0.996 ± 0.006	0.996 ± 0.004	0.996 ± 0.006	0.996 ± 0.004	0.996 ± 0.006
8	0.990 ± 0.010	0.991 ± 0.012	0.991 ± 0.009	0.992 ± 0.011	0.990 ± 0.010	0.991 ± 0.012	0.990 ± 0.010	0.991 ± 0.012
9	0.995 ± 0.004	0.995 ± 0.008	0.996 ± 0.004	0.995 ± 0.008	0.995 ± 0.004	0.995 ± 0.008	0.995 ± 0.004	0.995 ± 0.008

Table 4. Mean (μ) ± standard deviation (σ) of accuracy, precision, recall, and f1 score.

low training time. For example, the mean training time of F_d = 1 for scenario No. 1 (Fig. 12a) was 70937 s whereas that of F_d = 500 was 2168 s, which implies that high classification accuracy can be achieved with low computational cost. Note that the threshold F_d values in this study were evaluated between 500 and 1000, which can be altered by the number of sand types to be classified and the experimental setup.

Engineering implications

The accurate determination of the particle size is critical in estimating many geotechnical properties such as saturated hydraulic conductivity as inferred from the Kozeny-Carman equations[45,49,50], which shows that the saturated hydraulic conductivity is correlated to the square of particle size. Moreover, a precise assessment of d_{50} facilitates the estimation of various properties of sandy soils, including the range of void ratio[51] and relative density[52]. Furthermore, the estimation of d_{50} from the CNN model developed in this study can aid in predicting penetration resistance through various in-situ tests, such as the standard penetration test (SPT)–cone penetration test (CPT)[53], and dynamic cone penetration test[54], as the penetration resistance can be influenced by relative density, overburden pressure, and particle size[55]. For example, according to Robertson et al. (1983), the ratio of CPT cone tip resistance (q_c) to SPT N value corrected for 60% energy transfer ratio (N_{60}) can be expressed as a function of d_{50}:

$$\frac{\left(\frac{q_c}{p_a}\right)}{N_{60}} = 7.6429 \cdot \ {d_{50}}^{0.26} \tag{1}$$

where p_a denotes the atmospheric pressure. Equation (1) implies that the installation of a bender element in a cone[56] can provide the depth-dependent semi-continuous N_{60} values as d_{50} can be estimated from the pattern of bender element signals.

Another potential application of the developed framework can be monitoring the suffusion of gap-graded coarse-grained soils, which is important in the sustainable performance of earthen structures (e.g., dikes and levees)[57–59]. Specifically, the installation of the bender element at the suffusion susceptible regions provides the time series bender element signals, implying that the pattern of signals can be utilized to estimate the long-term variation of sand particle size using the developed framework unless bender elements are damaged. Therefore, it can be anticipated that the loss of small particles can be captured by chance in the pattern of signals, which eventually leads to the change in the predicted class in the developed CNN model. Even though a comprehensive investigation is still required to develop a reliable CNN model to classify the fine content of gap-graded coarse-grained soils to monitor the suffusion over time, the proposed framework suggests a high chance of monitoring suffusion using bender element signals combined with the CNN model.

According to[56], bender elements were used as field-embedded sensors to monitor the stiffness characteristics of airport pavement base courses. Thus, signals from bender elements detected at various layers can provide insights into changes in d_{50} and small-strain stiffness within localized zones. The applicability of the developed framework in the field can be more or less validated by classifying the sand as K1 sand using the signals obtained from the experimental setup for model validation shown in Fig. 4. The obtained signals during the penetration of the device well classified the sand type as K1 sand using the developed CNN models for nine scenarios. This validation result implies the high applicability of the developed framework for continuous estimation of d_{50} with depth at least for pure and homogeneous dry sand medium.

For evaluating small-strain stiffness and d_{50} of soil with depth, a field velocity probe with bender elements[60] and the developed framework can be used as shown in Fig. 13. Furthermore, the CNN model developed in this study can also be linked to the machine learning regression models with d_{50} as one of the input features to predict predictand (e.g., predicting permanent strain of soils[61]. Therefore, the developed framework in this study enables the estimation of the abovementioned geotechnical properties (e.g., d_{50}, hydraulic conductivity, N_{60}, and permanent strain) as a function of time and depth from real-time monitored bender element signals. As seen in Fig. 13, d_{50} of sand as a function of depth can be first estimated from the pattern of bender element signals, followed by the estimation of geotechnical properties using available empirical or theoretical models.

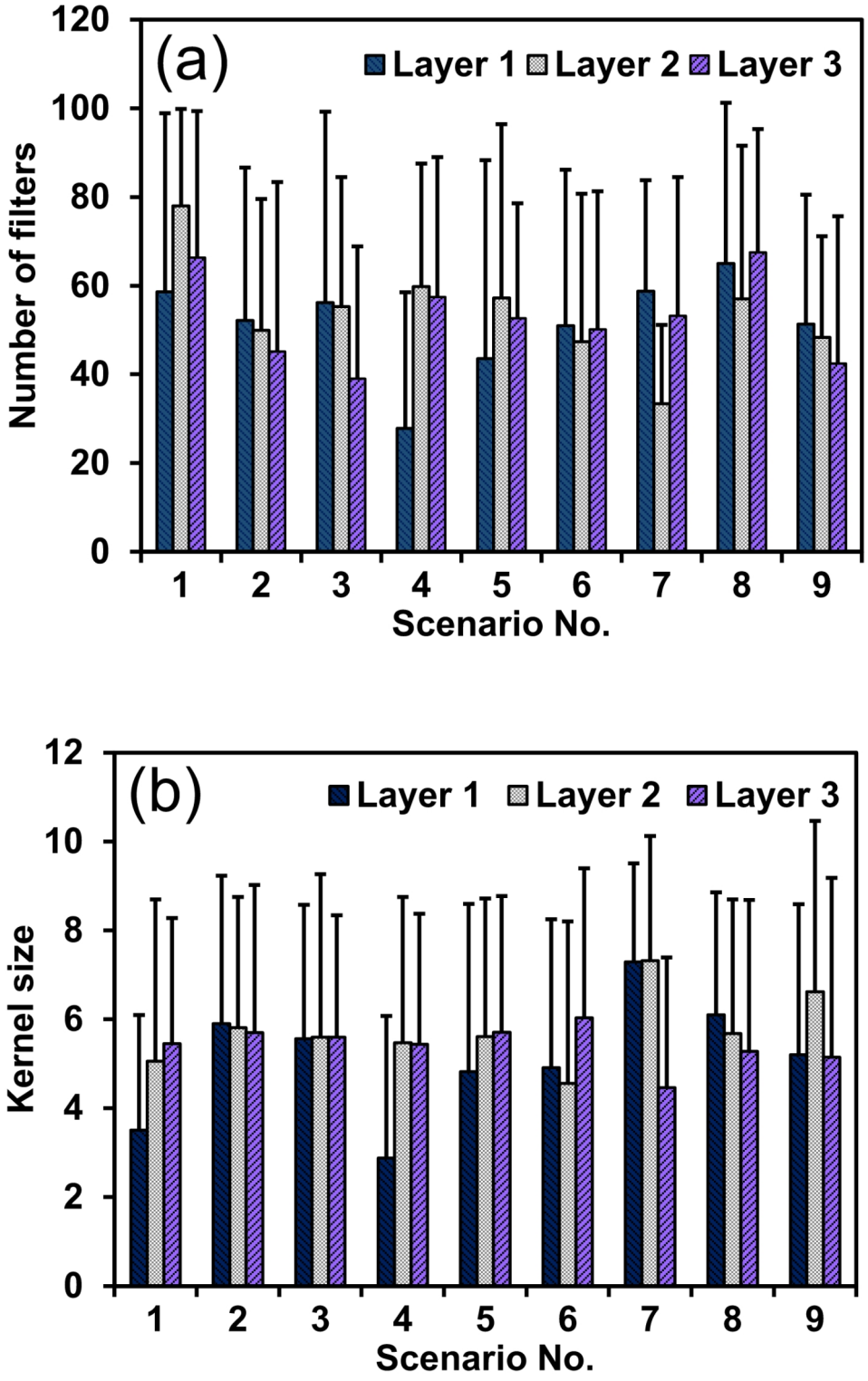

Fig. 10. Mean values of tuned number of filters (**a**) and kernel size (**b**) for 100 CNN models. Error bars represent the standard deviation of hyperparameters.

The limitation of the developed framework shown in this study is that laboratory experiments to construct a database are required for a reliable CNN model of target soils as the shear wave velocity is a function of many factors such as fine content, degree of saturation, and temperature[62–65]. Furthermore, because only uniform sand samples were used in this study, further study on the applicability of the developed framework to well-graded sand would be required. Nevertheless, the developed framework shown in this study indicates the chance of using the pattern of bender element signals in predicting the particle size of sand.

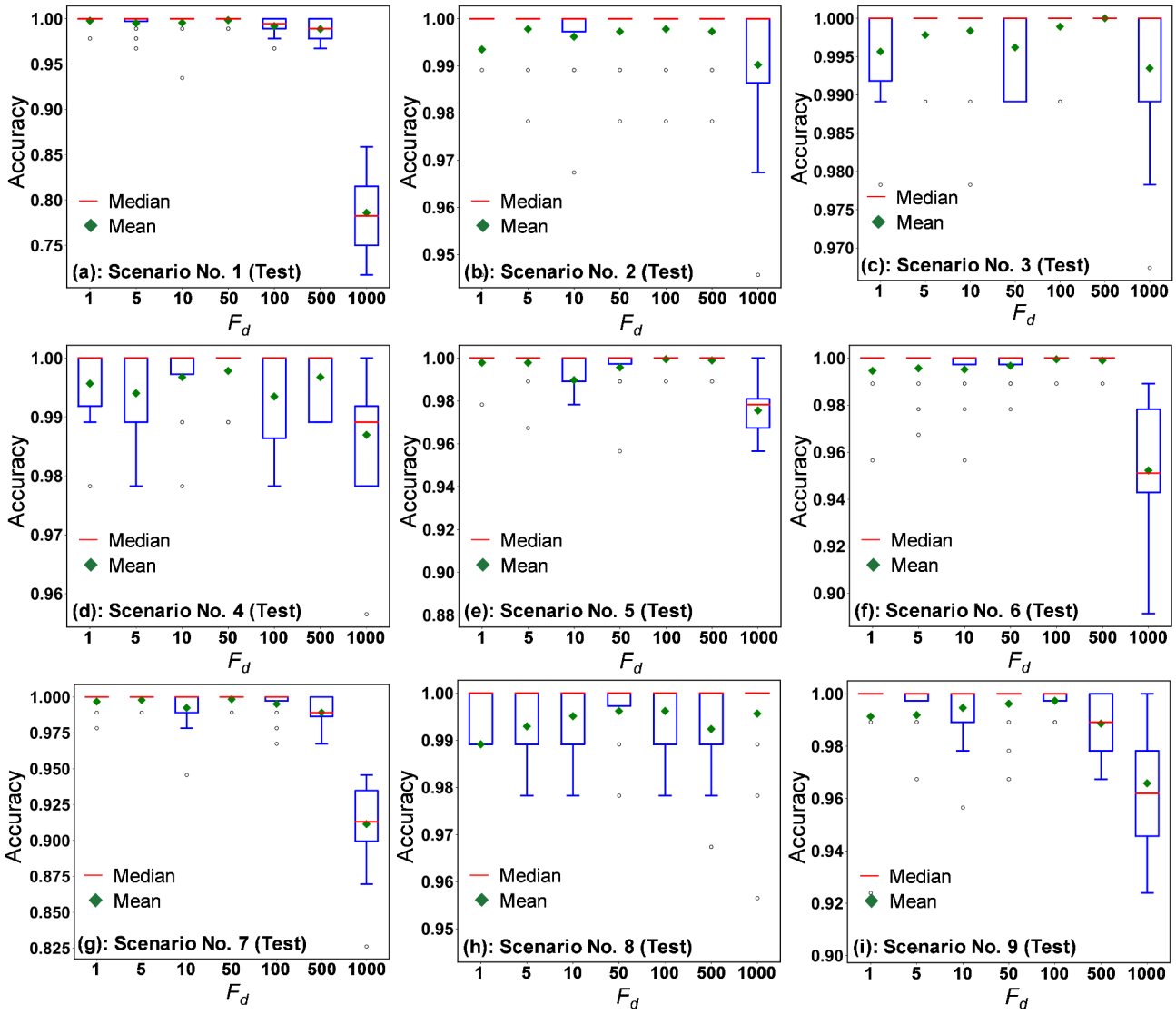

Fig. 11. Accuracy of 100 CNN models at F_d = 1, 5, 10, 50, 100, 600, and 1000 for the test dataset. The upper and lower bound of the box represents the 25th (Q1) and 75th percentile (Q3) and the upper and lower whisker represent Q1-1.5×IQR and Q3 + 1.5×IQR where IQR refers to Q3 – Q1. The outliers were illustrated as open-circle markers.

Conclusions

This study investigated the chance of applying CNN to detect the pattern of bender element signals for classifying sand particle size. Bender element signals for four types of sand with particle sizes ranging from 0.5 to 7 mm under vertical stresses of 10, 50, and 150 kPa and cutoff frequencies of 10, 50, and 100 kHz (a total of 9 scenarios) were obtained to train A one-dimensional CNN model. In addition, hyperparameter tuning was performed for 100 CNN models in each scenario to assess the repeatability and reliable performance of developed CNN models. The main findings from the developed framework are as follows:

1) The higher vertical stress resulted in increased resonant frequency and shorter first arrival times of shear waves, the pattern of bender element signals for a given type of sand was not significantly dependent on vertical stress and cutoff frequency.
2) The CNN models displayed high classification accuracy for sand types across all tested scenarios, implying that the developed CNN models well captured the different patterns of bender element signals as a function of sand type.
3) The high mean and low standard deviation of accuracy, precision, recall, and f1 score of 100 CNN models demonstrate the high performance of CNN models with good repeatability.
4) Relatively high variation of hyperparameters of CNN models reveals the need for tuning hyperparameters at a given train-test split as the accuracy of the CNN model increased from ~ 0.7 to 0.99 after hyperparameter tuning.

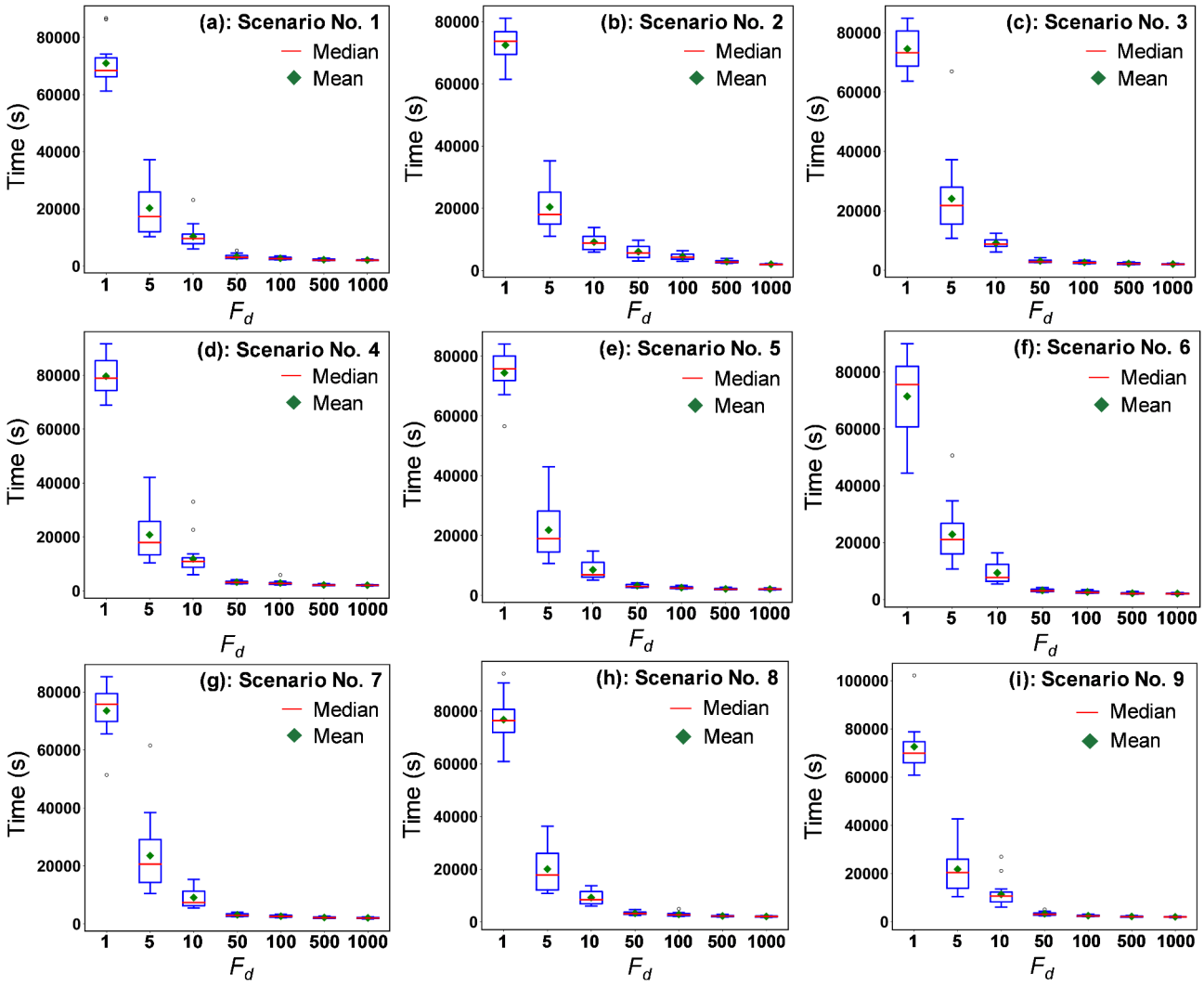

Fig. 12. Training time of 100 CNN models at F_d = 1, 5, 10, 50, 100, 600, and 1000.

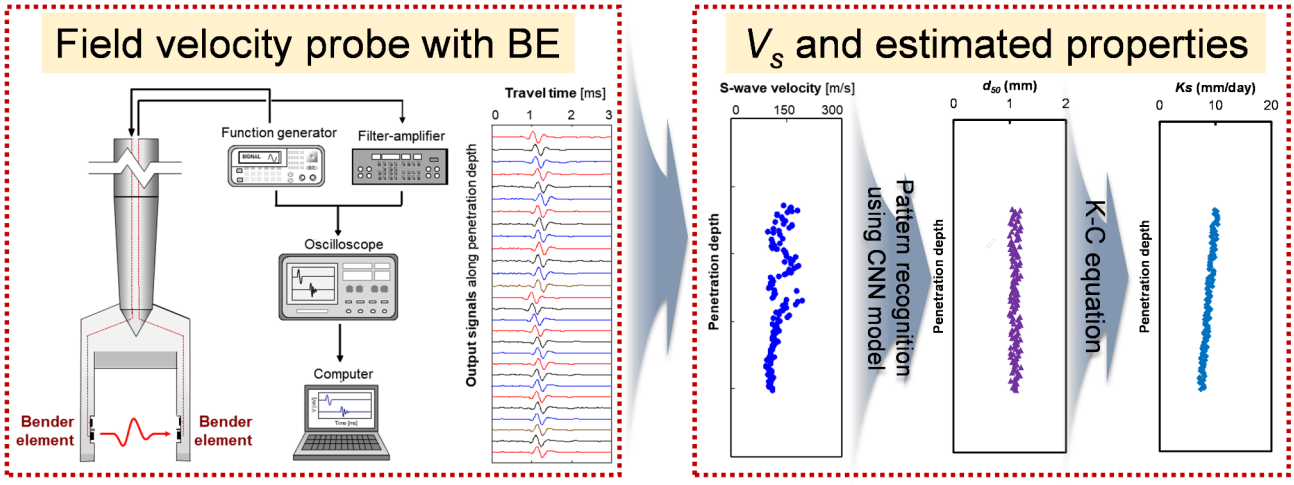

Fig. 13. Example application of the developed framework using field velocity probe.

5) The high accuracy for F_d = 500 (=9 data points in each dataset) was obtained in this study, implying that the low number of data (or low sampling rate) can also provide the CNN model with good accuracy.
6) The developed framework shown in this study can be used to predict time- and depth-dependent sand particle size and related geotechnical parameters (e.g., saturated hydraulic conductivity) using the monitored pattern of bender element signals.

Data availability

All data that support the findings of this study are available from the corresponding author (jwon@unist.ac.kr) upon reasonable request.

Received: 22 November 2024; Accepted: 20 February 2025
Published online: 26 February 2025

References

1. Shibuya, S., Hwang, S. C. & Mitachi, T. Elastic shear modulus of soft clays from shear wave velocity measurement. *Géotechnique* **47**, 593–601 (1997).
2. Kuwano, R. & Jardine, R. J. On the applicability of cross-anisotropic elasticity to granular materials at very small strains. *Géotechnique* **52**, 727–749 (2002).
3. Lee, C., Lee, J. S., Lee, W. & Cho, T. H. Experiment setup for shear wave and electrical resistance measurements in an oedometer. *Geotech. Test. J.* **31**, 149–156 (2008).
4. Byun, Y. H., Tran, K., Yun, M. S., Lee, J. S. & T. & Strength and stiffness characteristics of unsaturated hydrophobic granular media. *Geotech. Test. J.* **35**, 193–200 (2012).
5. Lee, J. S. & Santamarina, J. C. Seismic monitoring short-duration events: liquefaction in 1 g models. *Can. Geotech. J.* **44**, 659–672 (2007).
6. Yoon, H. K., Lee, J. S., Kim, Y. U. & Yoon, S. Fork blade-type field velocity probe for measuring shear waves. *Mod. Phys. Lett. B.* **22**, 965–969 (2008).
7. Byun, Y. H., Qamhia, I. I. A., Feng, B. & Tutumluer, E. Embedded shear wave transducer for estimating stress and modulus of As-constructed unbound aggregate base layer. *Constr. Build. Mater.* **183**, 465–471 (2018).
8. Byun, Y. H., Tutumluer, E., Feng, B., Kim, J. H. & Wayne, M. H. Horizontal stiffness evaluation of geogrid-stabilized aggregate using shear wave transducers. *Geotext. Geomembranes*. **47**, 177–186 (2019).
9. Kim, J. H. et al. American Society of Civil Engineers, Reston, VA,. Bender Element Shear Wave Measurement Based Local Stiffness Characteristics Related to Permanent Deformation Behavior of Geogrid-Stabilized Aggregate Specimens. In *Geo-Congress 2020* 517–526. https://doi.org/10.1061/9780784482810.054 (2020).
10. Kang, M., Wang, H., Qamhia, I. I. A. & Tutumluer, E. Modulus properties of granular materials at various strain levels from repeated load triaxial testing with Bender elements. In *Geo-Congress 2022 420–430 (American Society of Civil Engineers, Reston, VA*. https://doi.org/10.1061/9780784484067.042 (2022).
11. Gu, X., Zuo, K., Tessari, A. & Gao, G. Effect of saturation on the characteristics of P-wave and S-wave propagation in nearly saturated soils using Bender elements. *Soil. Dyn. Earthq. Eng.* **145**, 106742 (2021).
12. Ferreira, C., Díaz-Durán, F., da Fonseca, V., Cascante, G. & A. & New approach to concurrent VS and VP measurements using Bender elements. *Geotech. Test. J.* **44**, 1801–1820 (2021).
13. Won, J., Ryu, B. & Choo, H. Evolution of maximum shear modulus and compression index of rigid–soft mixtures under repetitive k < inf > 0 loading conditions. *Acta Geotech.* https://doi.org/10.1007/s11440-023-01945-x (2023).
14. Lee, J. S., Dodds, J. & Santamarina, J. C. Behavior of Rigid-Soft particle mixtures. *J. Mater. Civ. Eng.* **19**, 179–184 (2007).
15. Zhan, Y., Lu, S., Xiang, T. & Wei, T. Application of convolutional neural network in random structural damage identification. *Structures* **29**, 570–576 (2021).
16. Gulgec, N. S., Takáč, M. & Pakzad, S. N. Structural damage detection using convolutional neural networks. In 331–337. https://doi.org/10.1007/978-3-319-54858-6_33 (2017).
17. Gulgec, N. S., Takáč, M. & Pakzad, S. N. Convolutional neural network approach for robust structural damage detection and localization. *J. Comput. Civ. Eng.* **33**, (2019).
18. Li, M., Jia, D., Wu, Z., Qiu, S. & He, W. Structural damage identification using strain mode differences by the iFEM based on the convolutional neural network (CNN). *Mech. Syst. Signal. Process.* **165**, 108289 (2022).
19. Hsiao, C. H., Chen, A. Y., Ge, L. & Yeh, F. H. Performance of artificial neural network and convolutional neural network on slope failure prediction using data from the random finite element method. *Acta Geotech.* **17**, 5801–5811 (2022).
20. Fu, Y., Lin, M., Zhang, Y., Chen, G. & Liu, Y. Slope stability analysis based on big data and convolutional neural network. *Front. Struct. Civ. Eng.* **16**, 882–895 (2022).
21. Chen, G., Deng, W., Lin, M. & Lv, J. Slope stability analysis based on convolutional neural network and digital twin. *Nat. Hazards.* **118**, 1427–1443 (2023).
22. Oh, B. K., Park, Y. & Park, H. S. Seismic response prediction method for Building structures using convolutional neural network. *Struct. Control Heal Monit.* **27**, (2020).
23. Zhang, R., Liu, Y. & Sun, H. Physics-guided convolutional neural network (PhyCNN) for data-driven seismic response modeling. *Eng. Struct.* **215**, 110704 (2020).
24. Ng, W. et al. Convolutional neural network for simultaneous prediction of several soil properties using visible/near-infrared, mid-infrared, and their combined spectra. *Geoderma* **352**, 251–267 (2019).
25. Zhong, L., Guo, X., Xu, Z. & Ding, M. Soil properties: their prediction and feature extraction from the LUCAS spectral library using deep convolutional neural networks. *Geoderma* **402**, 115366 (2021).
26. Tsakiridis, N. L., Keramaris, K. D., Theocharis, J. B. & Zalidis, G. C. Simultaneous prediction of soil properties from VNIR-SWIR spectra using a localized multi-channel 1-D convolutional neural network. *Geoderma* **367**, 114208 (2020).
27. Samaei, M., Alinejad Omran, M., Keramati, M. & Naderi, R. Shirani Faradonbeh, R. Assessing the shear strength of sandy soil reinforced with polyethylene-terephthalate: an AI-based approach. *Earth Sci. Inf.* **17**, 4507–4526 (2024).
28. Zhu, L. et al. Prediction of soil shear strength parameters using combined data and different machine learning models. *Appl. Sci.* **12**, 5100 (2022).
29. Pham, B. T., Son, L. H., Hoang, T. A. & Nguyen, D. M. Tien Bui, D. Prediction of shear strength of soft soil using machine learning methods. *CATENA* **166**, 181–191 (2018).
30. Schaap, M. Using neural networks to predict soil water retention and soil hydraulic conductivity. *Soil. Tillage Res.* **47**, 37–42 (1998).
31. Pham, K., Kim, D., Le, C. V. & Won, J. Machine learning-based Pedotransfer functions to predict soil water characteristics curves. *Transp. Geotech.* **42**, (2023).
32. Pham, K. & Won, J. Enhancing the tree-boosting-based Pedotransfer function for saturated hydraulic conductivity using data preprocessing and predictor importance using game theory. *Geoderma* **420**, (2022).

33. Amiri Khaboushan, E., Emami, H., Mosaddeghi, M. R. & Astaraei, A. R. Estimation of unsaturated shear strength parameters using easily-available soil properties. *Soil. Tillage Res.* **184**, 118–127 (2018).
34. Liu, L., Yang, Y., Mao, X. & Nie, M. Macro-meso shear properties of alluvial-diluvial soil-rock mixture (ADSRM) subgrade fillers based on field investigation and N-method. *Case Stud. Constr. Mater.* **17**, e01694 (2022).
35. Usowicz, B. & Lipiec, J. Spatial variability of saturated hydraulic conductivity and its links with other soil properties at the regional scale. *Sci. Rep.* **11**, 8293 (2021).
36. Boadu, F. K. Hydraulic conductivity of soils from Grain-Size distribution: new models. *J. Geotech. Geoenvironmental Eng.* **126**, 739–746 (2000).
37. Wang, J., François, B. & Lambert, P. Equations for hydraulic conductivity Estimation from particle size distribution: A dimensional analysis. *Water Resour. Res.* **53**, 8127–8134 (2017).
38. Zhai, Q., Rahardjo, H., Satyanaga, A. & Dai, G. Estimation of the soil-water characteristic curve from the grain size distribution of coarse-grained soils. *Eng. Geol.* **267**, 105502 (2020).
39. Lee, J. S. & Santamarina, J. C. Bender elements: performance and signal interpretation. *J. Geotech. Geoenvironmental Eng.* **131**, 1063–1070 (2005).
40. Wang, Y. H., Lo, K. F., Yan, W. M. & Dong, X. B. Measurement biases in the Bender element test. *J. Geotech. Geoenvironmental Eng.* **133**, 564–574 (2007).
41. Lo, S. C. B. et al. Artificial Convolution neural network for medical image pattern recognition. *Neural Netw.* **8**, 1201–1214 (1995).
42. Traore, B. B., Kamsu-Foguem, B. & Tangara, F. Deep Convolution neural network for image recognition. *Ecol. Inf.* **48**, 257–268 (2018).
43. Kim, Y. & Yun, T. S. Enhanced rock mass rating prediction from tunnel face imagery: A decision-supportive ensemble deep learning approach. *Eng. Geol.* **339**, 107625 (2024).
44. Park, J., Kim, Y., Kim, S. S., Kim, K. Y. & Yun, T. S. Effect of injection rate and viscosity on stimulated fracture in granite: extraction of fracture by convolutional neural network and morphological analysis. *Rock. Mech. Rock. Eng.* **57**, 2159–2174 (2024).
45. Sung, Y., Lim, G., Kim, H. K., Won, J. & Choi, H. J. A novel approach to estimate sand particle-size using convolutional neural network with acoustic sensing. *Catena* **234**, (2024).
46. Lim, H. G. et al. Automated classification of clay suspension using acoustic sensing combined with convolutional neural network. *Min. Eng.* **202**, 108261 (2023).
47. Bagnall, A., Lines, J., Bostrom, A., Large, J. & Keogh, E. The great time series classification bake off: a review and experimental evaluation of recent algorithmic advances. *Data Min. Knowl. Discov.* **31**, 606–660 (2017).
48. Byun, Y. H., Han, W., Tutumluer, E. & Lee, J. S. Elastic wave characterization of controlled low-strength material using embedded piezoelectric transducers. *Constr. Build. Mater.* **127**, 210–219 (2016).
49. Carrier, W. D., Goodbye, H. & Hello, K. C. *J. Geotech. Geoenvironmental Eng.* **129**, 1054–1056 (2003).
50. Won, J., Park, J., Choo, H. & Burns, S. Estimation of saturated hydraulic conductivity of coarse-grained soils using particle shape and electrical resistivity. *J. Appl. Geophys.* **167**, (2019).
51. Cubrinovski, M. & Ishihara, K. Empirical correlation between SPT N-Value and relative density for sandy soils. *Soils Found.* **39**, 61–71 (1999).
52. Patra, C., Sivakugan, N., Das, B. & Rout, S. Correlations for relative density of clean sand with median grain size and compaction energy. *Int. J. Geotech. Eng.* **4**, 195–203 (2010).
53. Robertson, P. K., Campanella, R. G. & Wightman, A. SPT-CPT correlations. *J. Geotech. Eng.* **109**, 1449–1459 (1983).
54. Lee, C., Kim, K. S., Woo, W. & Lee, W. Soil stiffness gauge (SSG) and dynamic cone penetrometer (DCP) tests for estimating engineering properties of weathered sandy soils in Korea. *Eng. Geol.* **169**, 91–99 (2014).
55. Skempton, A. W. Standard penetration test procedures and the effects in sands of overburden pressure, relative density, particle size, ageing and overconsolidation. *Géotechnique* **36**, 425–447 (1986).
56. Kang, X., Sun, H. M., Luo, H., Dai, T. & Chen, R. P. A portable Bender Element-Double cone penetration testing equipment for measuring stiffness and shear strength of In-Situ soft soil deposits. *KSCE J. Civ. Eng.* **24**, 3546–3560 (2020).
57. Won, J., Choe, Y., Yang, Y. & Choi, H. Impact of clay particle reattachment on suffusion of sand-clay mixtures. *J. Rock. Mech. Geotech. Eng.* **15**, (2023).
58. Choe, Y., Choi, H. & Won, J. Suffusion of a sand–clay mixture: impact of the ionic-concentration gradient, clay type, sand-grain size and hydraulic gradient. *Géotechnique* 1–15. https://doi.org/10.1680/jgeot.21.00335 (2022).
59. Won, J., Kim, T., Kang, M., Choe, Y. & Choi, H. Suffusion of sand–clay mixture by three-staged change of ionic strength. *Can. Geotech. J.* **59**, (2022).
60. Yoon, H. K. & Lee, J. S. Field velocity resistivity probe for estimating stiffness and void ratio. *Soil. Dyn. Earthq. Eng.* **30**, 1540–1549 (2010).
61. Won, J., Tutumluer, E. & Byun, Y. H. Predicting permanent strain accumulation of unbound aggregates using machine learning algorithms. *Transp. Geotech.* **42**, (2023).
62. Kim, B. K., Lee, J. S., Park, J. & Kim, S. Y. Response of sand added with various biopolymer contents under repetitive loading and freeze–thaw cycles. *Transp. Geotech.* **47**, 101280 (2024).
63. Leong, E. C. & Cheng, Z. Y. Effects of confining pressure and degree of saturation on wave velocities of soils. *Int. J. Geomech.* **16**, (2016).
64. Akbari Paydar, N. & Ahmadi, M. M. Effect of fines type and content of sand on correlation between shear wave velocity and liquefaction resistance. *Geotech. Geol. Eng.* **34**, 1857–1876 (2016).
65. Yang, J. & Liu, X. Shear wave velocity and stiffness of sand: the role of non-plastic fines. *Géotechnique* **66**, 500–514 (2016).

Acknowledgements

This study was funded by National Research Foundation of Korea (NRF) grants funded by the Korean government (MSIT) (RS-2023-00221719 and RS-2022-NR071877).

Author contributions

J.W. and Y.-H. B. wrote the main manuscript text and drawing figures, J.I.S. performed bender element experiments, H.C. contributes funding acquisition and supervised the research and J.Y. construct CNN models presented in this study. All authors reviewed the manuscript.

Declarations

Competing interests

The authors declare no competing interests.

Additional information

Correspondence and requests for materials should be addressed to J.W.

Reprints and permissions information is available at www.nature.com/reprints.

Publisher's note Springer Nature remains neutral with regard to jurisdictional claims in published maps and institutional affiliations.